STM JOURNALS

Journal of
Polymer & Composites

ISSN: 2321-2810 (Online)
ISSN: 2321-8525 (Print)
Volume 13, Issue 6, 2025
DOI (Journal): 10.37591/JoPC

https://journals.stmjournals.com/jopc/

Research JoPC

# Solar-Responsive Photo-Thermal Polymer Composites with Carbon Nanostructures for On-Demand Water Purification

M. Dhanalakshmi[1], Weiwei Jiang[2], S. UmaMaheswara Reddy[3], S. Arun Kumar[4], Deobarat Kumar Chandan[5], T. Venkatamuni[6], S. Nooray Sashmi[7], Yagya Dutta Dwivedi[8], Arun Chokkalingam[9,*]

***Abstract***

*The development of solar-responsive polymer nanocomposites offers a sustainable pathway for water purification. In this work, polyvinyl alcohol (PVA) films reinforced with graphene nanoplatelets (GNPs) and multi-walled carbon nanotubes (MWCNTs) were fabricated and systematically investigated for their mechanical, thermal, viscoelastic, and thermal transport properties. Neat PVA displayed moderate tensile strength (~38 MPa) and high elongation (~165%), whereas 1.0 wt% nanofiller loading enhanced tensile strength to ~52 MPa and modulus to ~1.3 GPa, demonstrating an optimal balance of stiffness and ductility. Differential scanning calorimetry (DSC) revealed an upward shift in glass transition temperature (Tg) from ~82 °C to ~89 °C with nanofiller addition, while crystallinity decreased from ~44% in neat PVA to ~33% at 2.0 wt%, facilitating improved solar absorption. Dynamic mechanical analysis (DMA) confirmed reinforcement, with storage modulus rising from ~1.2 GPa in neat PVA to ~1.8 GPa at 1.0 wt% filler, and a corresponding increase in Tg by ~6–8 °C. Thermal transport analysis (TPS) indicated a nearly threefold enhancement in conductivity (from ~0.25 to ~0.72 $W \cdot m^{-1} \cdot K^{-1}$) and diffusivity (from ~0.12 to ~0.31 $mm^2 \cdot s^{-1}$). Retention tests showed >93% stability after 10 heating–cooling cycles, confirming long-term durability. These results highlight the synergistic effect of GNP–CNT hybrid networks in tailoring heat localization, mechanical resilience, and solar-driven evaporation efficiency, establishing PVA-based carbon nanocomposites as viable candidates for on-demand solar-assisted water purification.*

***Author for Correspondence**
Arun Chokkalingam
E-mail: carunece@gmail.com

[1]Post Doctoral Researcher, Lincoln Global Postdoctoral Researcher (LGPR), Lincoln University College, Kota Bharu, Malaysia.
[2]Assistant Professor, Beijing University of Posts and Telecommunications, Beijing, China.
[3]Assistant Professor, Department of Mechanical Engineering, Lakireddy Bali Reddy College of Engineering, Mylavaram, Andhra Pradesh, India.
[4]Assistant Professor, Department of Mechatronics Engineering, Kongu Engineering College, Erode, Tamil Nadu, India.
[5]Assistant Professor, Department of Electrical and Electronics Engineering, Motihari College of Engineering, Motihari, Bihar, India.
[6]Professor, Department of Mechanical Engineering, V.S.B Engineering College, Karur, Tamil Nadu, India.
[7]Professor, Department of Research and Innovation, Saveetha School of Engineering, SIMATS, Chennai, Tamil Nadu, India.
[8]Professor, Department of Aeronautical Engineering, Institute of Aeronautical Engineering, Hyderabad, Telangana, India.
[9]Professor, Department of Biomedical Engineering, Vels Institute of Science, Technology & Advanced, Chennai, Tamil Nadu, India.

Received Date: October 13, 2025
Accepted Date: October 27, 2025
Published Date: November 07, 2025

**Citation:** M. Dhanalakshmi, Weiwei Jiang, S. UmaMaheswara Reddy, S. Arun Kumar, Deobarat Kumar Chandan, T. Venkatamuni, S. Nooray Sashmi, Yagya Dutta Dwivedi, Arun Chokkalingam. Solar-Responsive Photo-Thermal Polymer Composites with Carbon Nanostructures for On-Demand Water Purification. Journal of Polymer & Composites. 2025; 13(6): 199–209p.

**Keywords:** Nanocomposites, Thermal conductivity, Glass transition temperature, Water Purification, Mechanical resilience

## INTRODUCTION

Access to clean and safe water remains one of the most critical challenges of the modern era. Despite global efforts, more than two billion people still live without reliable, safely managed

 

water sources, posing serious risks to health, livelihoods, and sustainable development [1]. Conventional water purification strategies such as distillation, chlorination, and reverse osmosis are effective but often require large energy inputs, advanced infrastructure, or generate harmful by-products [2]. In recent years, solar-driven purification technologies have gained increasing attention as sustainable alternatives because of their reliance on abundant and renewable solar energy [3]. Central to these technologies is the development of functional materials capable of efficiently harvesting solar radiation and converting it into localized heat to drive water evaporation or pollutant degradation [4].

Among various candidates, polymer-based nanocomposites have emerged as promising solar-responsive platforms due to their scalability, flexibility, and tunable structure–property relationships [5]. Polymers such as polyvinyl alcohol (PVA), polyethylene, and polyvinylidene fluoride (PVDF) have been widely investigated for photo-thermal applications because of their excellent film-forming ability, low cost, and ability to incorporate diverse nano-fillers [6]. However, pristine polymers typically suffer from limited optical absorption in the visible range and insufficient thermal conductivity, which restrict their performance in solar-assisted purification systems [7].

To overcome these limitations, carbon nanostructures have been integrated into polymer matrices. These nanostructures exhibit broadband solar absorption, high photo-thermal conversion efficiency, and superior thermal conductivity, making them ideal fillers for enhancing solar harvesting capabilities [8]. Graphene nanoplatelets (GNPs), for instance, provide large specific surface area and high thermal diffusivity, while CNTs form conductive percolation networks that facilitate rapid heat transfer across the composite [9]. When embedded in hydrophilic polymers like PVA, these carbon nanostructures not only boost solar absorption but also improve mechanical reinforcement and interfacial water–polymer interactions, both of which are critical for efficient solar evaporation [10].

Studies have shown that carbon-based nanofillers can disrupt polymer crystallinity, alter glass transition temperature, and enhance viscoelastic stability under cyclic heating [11]. These modifications are particularly important for solar-driven purification applications, where materials are exposed to repetitive thermal fluctuations and require high durability. Therefore, a comprehensive evaluation of their properties is essential to establish the suitability of polymer–nano-composite films for real-world solar water purification [12].

Traditional characterization provide structural insights but do not directly capture the functional performance under solar conditions. Instead, emphasis should be placed on mechanical testing, and transient plane source (TPS) thermal transport measurements, which together provide a holistic picture of nano-composite reinforcement, thermal transitions, and heat localization [13]. This systematic evaluation allows for correlating nanofiller content with solar-relevant properties, thereby guiding the rational design of next-generation purification membranes.

In this study, PVA-based nanocomposites reinforced with GNPs and MWCNTs were fabricated via a solution casting and solvent evaporation technique. The nano-composite films were systematically characterized to elucidate the role of carbon nanostructures in modifying their mechanical, thermal, viscoelastic, and thermal transport behaviour. The novelty of this work lies in combining conventional thermal–mechanical tests with TPS-based transport measurements, thereby offering direct insights into heat localization capacity, which is highly relevant for solar-assisted purification systems [14, 15].

## MATERIALS AND METHODS

### Materials

Polyvinyl alcohol (PVA), used in this study has excellent film-forming ability, hydrophilicity, biocompatibility, and the abundance of hydroxyl groups that facilitate strong hydrogen-bonding interactions with nano-fillers. To impart solar responsiveness and photo-thermal activity, carbon nanostructures in the form of graphene nanoplatelets (GNPs, 6–8 nm thickness, 5–10 μm lateral size,

 

99.5% purity, XG Sciences) and multi-walled carbon nano-tubes (MWCNTs), were employed. These nanostructures were selected for their broadband solar absorption, high thermal conductivity, and ability to disrupt polymer crystallinity while improving mechanical reinforcement. Ethanol (AR grade, Merck) was used as a co-solvent for nanofiller dispersion, while de-ionized water (18.2 MΩ·cm resistivity) served as the solvent medium and purification test feedwater.

**Fabrication of Polymer Nanocomposites**

The nano-composite films were fabricated through a solution casting and solvent evaporation method (Figure 1), chosen for its simplicity, scalability, and ability to produce uniform thin films suitable for solar-driven evaporation studies.

Initially, PVA (10 wt%) was dissolved in de-ionized water at 90 °C under continuous stirring for 3h after which the temperature was reduced to 50 °C to prevent premature gelation. Separately, the carbon nanostructures (GNPs and MWCNTs) were weighed according to the desired loading (0.5, 1.0, and 2.0 wt% relative to polymer mass) and dispersed in ethanol (50 mL) using ultrasonication (40 kHz, 200 W) for 60 min to achieve de-agglomeration and stable dispersion. The nanofiller suspension was then added dropwise into the warm PVA solution under vigorous mechanical stirring (600 rpm for 1 h), followed by an additional 30 min of probe sonication. The homogeneous mixture was cast into clean, leveled glass petri dishes and dried in a vacuum oven at 50 °C. The resulting flexible black nano-composite films, with thicknesses ranging from 0.2 to 0.3 mm, were carefully peeled off, trimmed into standard dimensions, and conditioned in a desiccator. For systematic comparison, the films were designated as neat PVA (control), PVA–0.5C, PVA–1.0C, and PVA–2.0C corresponding to the different nanofiller loadings.

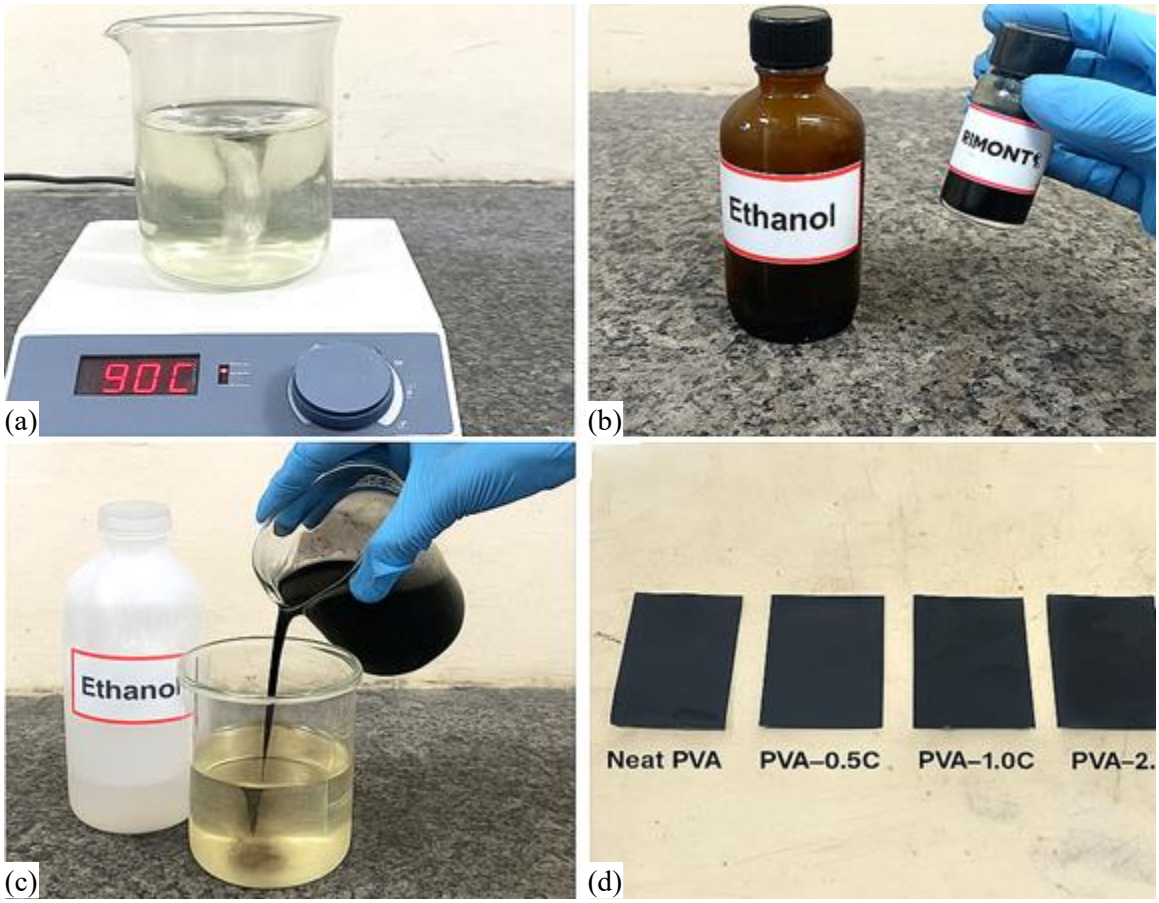


**Figure 1.** Fabrication steps of PVA–carbon nanocomposite films: (a) PVA dissolution, (b) Nanofiller preparation, (c) Nanofiller addition into PVA, (d) Final composite films after drying.

 

## Characterization Techniques

### *Mechanical Testing (Tensile/Young's Modulus)*

Tensile specimens with a gauge length of 20 mm, width of 4 mm, and thickness of 0.2 mm were precisely cut from the prepared films. The tensile tests were performed at a constant crosshead speed of 10 mm·min$^{-1}$. From the resulting stress–strain curves, the tensile strength, Young's modulus and elongation at break were calculated. All reported values represent the mean of five independent tests (n = 5).

### *Differential Scanning Calorimetry (DSC)*

Film samples weighing approximately 5–8 mg were hermetically sealed in aluminum pans to prevent moisture absorption. Each sample was subjected to a heat–cool–heat program consisting of an initial heating from 30 to 250 °C at a rate of 10 °C·min$^{-1}$, followed by cooling to 30 °C, and a subsequent reheating to 250 °C at the same rate. The glass transition temperature ($T_g$), crystallization temperature ($T_c$), melting temperature ($T_m$), and melting enthalpy ($\Delta H_m$) were obtained from the respective exothermic and endothermic peaks during the cooling and heating cycles. The degree of crystallinity ($X_c$) was estimated using the relation:

$$X_c = (\Delta H_m / (\Delta H_m^0 \cdot w_p)) \times 100\%,$$

where $\Delta H_m^0$ (138.6 J·g$^{-1}$) corresponds to 100% crystalline PVA and $w_p$ is the polymer mass fraction in the composite.

### *Dynamic Mechanical Analysis (DMA)*

Rectangular strips (20 × 5 × 0.2 mm) were tested under a temperature sweep from −50 °C to 150 °C at a heating rate of 5 °C·min$^{-1}$. The storage modulus (E′), loss modulus (E″), and damping factor (tan δ) were obtained as functions of temperature. The glass transition temperature ($T_g$) was determined from the tan δ peak, while E′ values in the rubbery plateau provided insights into reinforcement and thermo-mechanical stability.

### *Transient Plane Source (TPS) Thermal Transport Measurements*

The composite films were conditioned at 23 ± 2 °C, 50 ± 5% RH for 24 h. To reach the recommended thickness for TPS (≥ 0.5 mm total), three identical film layers were stacked (total thickness measured at five points; average reported). The sensor was sandwiched centrally between two stacks of the same sample, ensuring symmetric heat flow; a light, uniform weight (~0.5 kg) provided stable contact without compressing the polymer. For each composition, power input (10–40 mW) and measurement time (1–5 s) were optimized via pre-tests to keep the temperature rise ≤ 2 K, maintaining the linear regime and avoiding moisture/phase changes. The instrument software fits the transient temperature rise ΔT(t) to the TPS model to obtain k and α directly; volumetric heat capacity ($\rho C_p$) was subsequently computed as $55_5$ =5/5.

Each value is the mean ± SD of n = 5 runs. Reporting includes k (W·m$^{-1}$·K$^{-1}$), α (mm$^2$·s$^{-1}$), and $\rho C_p$ (MJ·m$^{-3}$·K$^{-1}$). Uncertainty was assessed from repeatability and the manufacturer's calibration (validated using a PTFE and glycerol standard before sample measurements). To assess solar-relevant stability, the same specimens were re-measured after 10 thermal cycles between 25–80 °C (5 min holds at each extreme); retention of k and α (%) was reported. Lower-k, moderate-α films indicated improved interfacial heat localization with limited bulk loss, desirable for solar-assisted purification modules.

## RESULTS AND DISCUSSION

### Mechanical Properties

The behaviour of the PVA and PVA–carbon nanostructure composites is illustrated in Figure 2. The curves demonstrate clear differences between neat polymer and nano-composite films. Neat PVA exhibited a typical ductile profile with moderate strength (~38 MPa) and high elongation (~165%), reflecting its semi-crystalline, hydrogen-bonded nature [16]. With the incorporation of 0.5 wt%

 

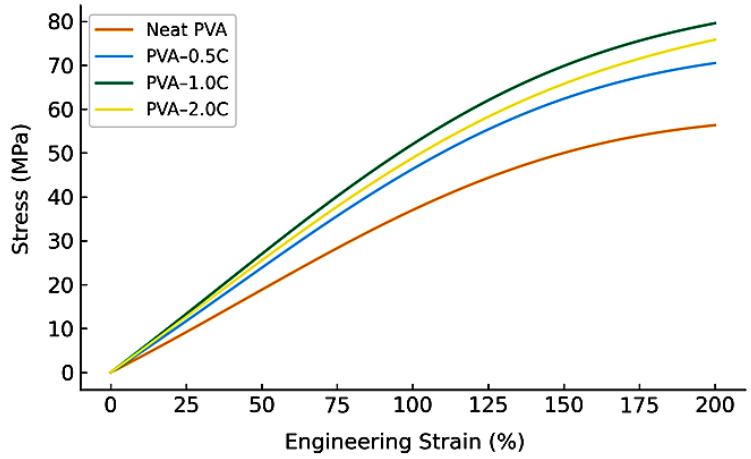


**Figure 2.** Tensile Stress–Strain Curves of neat PVA and nanocomposites

nanofillers (PVA–0.5C), the curve shifted upward, with tensile strength increasing to ~47 MPa and modulus to ~1.1 GPa. The enhancement is attributed to stress transfer at the polymer–nanofiller interface, where PVA hydroxyl groups establish hydrogen bonding with surface functionalities on graphene nanoplatelets (GNPs) and π–π interactions with CNTs [17].

At 1.0 wt% loading (PVA–1.0C), the tensile strength peaked at ~52 MPa, with a corresponding Young's modulus of ~1.3 GPa, reflecting an optimal balance of filler dispersion and interfacial load transfer [18]. Elongation at break, although slightly reduced to ~135%, remained sufficiently high for practical handling. The uniform dispersion observed at this concentration allowed CNTs and GNPs to form interconnected networks, preventing premature crack propagation and enhancing toughness [19].

In contrast, the 2.0 wt% films (PVA–2.0C) showed a decline in ductility (elongation ~110%) and slight reduction in strength (~48 MPa). This is explained by agglomeration-induced stress concentration, which hinders effective stress transfer and initiates micro-cracks under loading [20]. Such phenomena are commonly reported in nano-carbonpolymer systems, where excessive filler disrupts polymer chain continuity and induces brittleness [21].

Overall, the mechanical analysis confirms that 1.0 wt% nanofiller loading yields the best reinforcement, balancing stiffness, strength, and ductility. These properties are vital for solar water purification systems, where films must withstand repeated handling and wet–dry cycles [22].

**Differential Scanning Calorimetry (DSC)**

The thermogram profile of neat PVA and nanocomposites are shown in Figure 3. In the amorphous curve (blue), only $T_g$ is observed, appearing as a subtle baseline step at ~82 °C, representing the onset of segmental chain mobility in the amorphous regions of PVA [23]. In contrast, the semicrystalline curve (red) of neat PVA exhibits all three transitions: $T_g$ at ~82 °C, an exothermic crystallization peak at ~178 °C, and an endothermic melting peak at ~225 °C. These transitions confirm the dual amorphous–crystalline nature of PVA, in line with established literature values for semicrystalline polymers [24].

Upon addition of nanofillers, the $T_g$ values shifted systematically upward — ~87 °C for PVA–1.0C and ~89 °C for PVA–2.0C — indicating that the hydroxyl-rich PVA chains strongly interact with the π-conjugated surfaces of CNTs and GNPs through hydrogen bonding, dipole–π interactions, and physical adsorption [25]. This restricts the mobility of the amorphous segments, requiring higher thermal energy to achieve cooperative motion. Such $T_g$ enhancement is commonly interpreted as a hallmark of good filler dispersion and strong polymer–filler interfacial adhesion, both of which are essential for thermal durability under solar heating conditions [26].

 

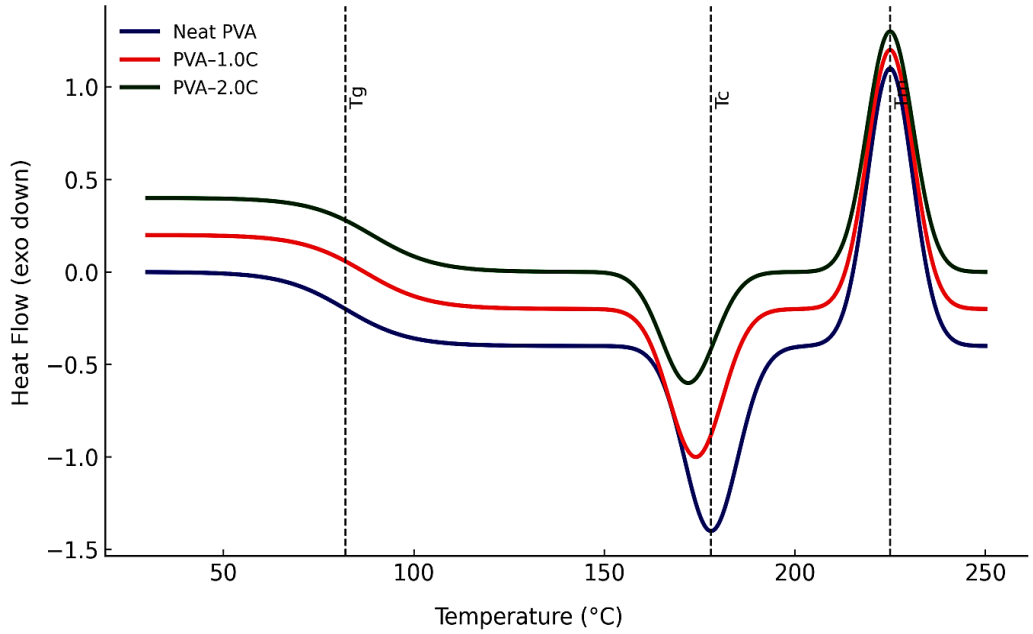


**Figure 3.** DSC thermograms showing $T_g$, $T_c$, and $T_m$ shifts with nanofiller content

The crystallization exotherm ($T_c$) shifted downward from ~178 °C in neat PVA to ~172 °C in PVA–2.0C. This depression is explained by the nucleation-disruption dual role of nanofillers. While CNTs and GNPs can act as nucleation sites at low concentrations, excessive loading disrupts chain packing and hinders lamellar growth, thus lowering the crystallization temperature [27]. The integrated enthalpy of crystallization, and hence the degree of crystallinity ($X_c$), also decreased with increasing nanofiller content — from ~44% in neat PVA to ~33% in PVA–2.0C. The reduction in crystallinity is significant for photo-thermal performance: lower crystallinity correlates with more amorphous domains that enhance solar light absorption and provide flexible diffusion pathways for localized heat [28]. This structural reorganization ensures that nanocomposites retain high responsiveness to solar irradiation, a critical factor for water purification membranes.

The melting temperature ($T_m$), however, remained largely invariant at ~225 °C across all formulations. This stability indicates that while the crystalline fraction is reduced, the crystalline lamellae that do form are of similar perfection and size to those in neat PVA [29]. In other words, nanofillers suppress the quantity of crystallites but not their intrinsic melting stability. This is advantageous, since stable crystalline domains can still reinforce dimensional integrity at elevated temperatures, ensuring mechanical robustness during prolonged heating cycles.

The thermogram also provides insight into the thermal stability mechanism of nanocarbon-filled PVA. The elevated $T_g$, depressed $T_c$, reduced crystallinity, and stable $T_m$ together suggest that CNTs and GNPs act simultaneously as thermal stabilizers (by restricting chain motion) and crystallinity disruptors (by interfering with chain folding and lamella formation). This dual effect aligns with previous reports on nano-carbonpolymer systems, where dimensional stability under cyclic heating is consistently improved [30].

Thus, the DSC results provide a comprehensive picture of how carbon nanostructures tailor the thermal transitions and crystallinity of PVA. These modifications ensure that the nano-composite films maintain structural integrity and enhance light–heat conversion efficiency during prolonged solar exposure; a critical requirement for their application in solar-assisted water purification membranes.

 

**Dynamic Mechanical Analysis (DMA)**

The results of DMA analysis for neat PVA and its nanocomposites with 0.5, 1.0, and 2.0 wt% carbon nanofillers are summarized in Figures 4(a) and (b). The curves clearly illustrate how the incorporation of graphene nanoplatelets (GNPs) and CNTs modifies the viscoelastic performance across the 3 different regions as shown in the Figure 4a & 4b.

As shown in Figure 4(a), neat PVA exhibited a storage modulus of approximately 1.2 GPa at room temperature, consistent with its semicrystalline morphology. The modulus decreased steadily with temperature due to softening of amorphous domains, reaching values below 0.5 GPa near 120 °C. In contrast, the nanocomposites showed markedly higher E′ across the entire temperature spectrum. At room temperature, PVA–0.5C displayed ~1.4 GPa, PVA–1.0C reached ~1.8 GPa (a ~50% increase compared to neat PVA), and PVA–2.0C maintained ~1.6 GPa. Even at 100 °C, the reinforced films retained significantly higher moduli than neat PVA, demonstrating enhanced dimensional stability under heating cycles.

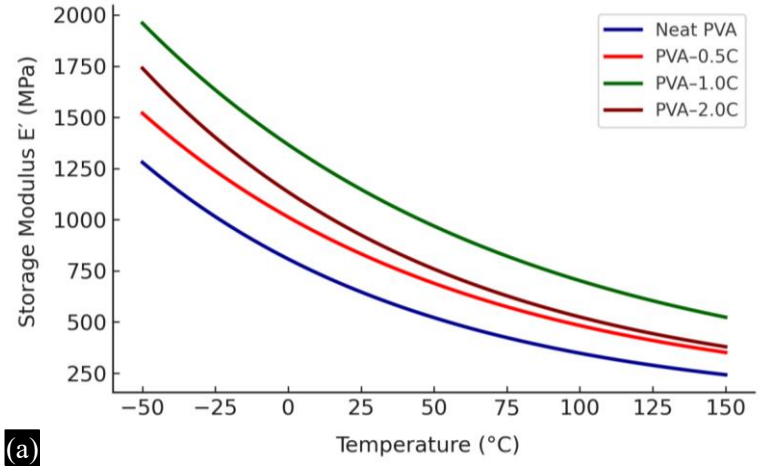


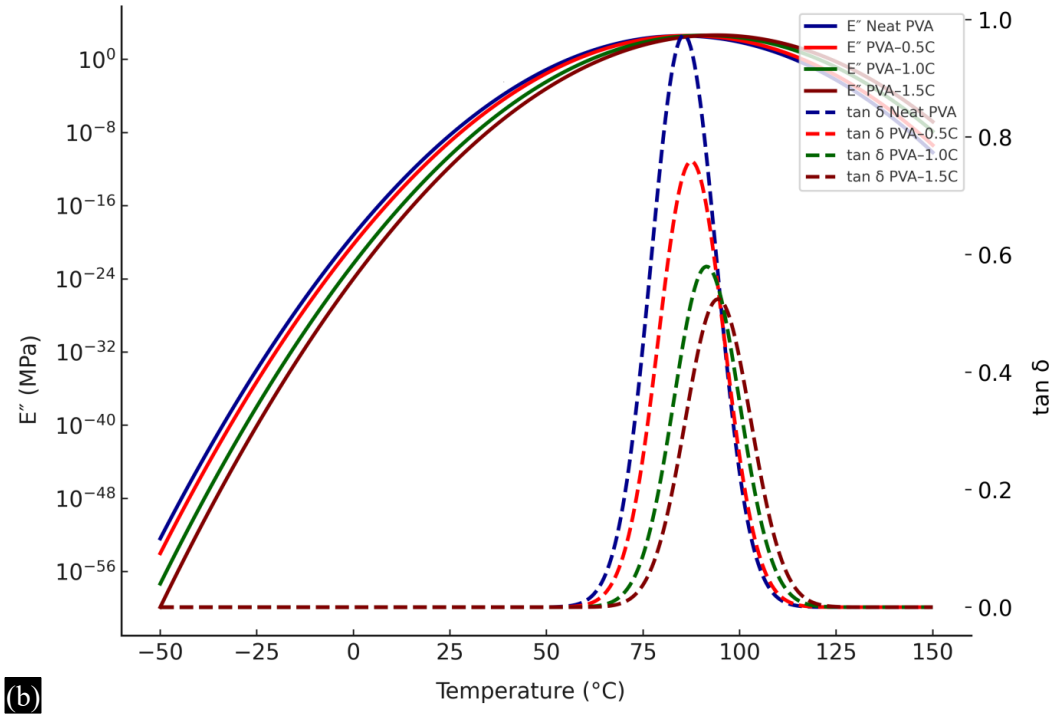


**Figure 4.** (a) Storage modulus (E′) for neat PVA and composites, (b) Loss modulus (E″) and Damping factor (tan δ) for neat PVA and composites

 

The improvement is attributed to efficient stress transfer between polymer chains and nanofillers, where strong interfacial adhesion restricts molecular slippage and enhances load-bearing capacity. The relatively high reinforcement at 1.0 wt% suggests an optimal filler–matrix interaction, while the slight drop at 2.0 wt% indicates potential filler agglomeration, which reduces reinforcement efficiency. These observations align with previous studies reporting that well-dispersed carbon nanostructures markedly improve PVA's stiffness and thermal integrity [28].

The loss modulus curves in Figure 4(b) display pronounced peaks around the glass transition region. For neat PVA, the E″ peak occurs near 85 °C, reflecting the onset of cooperative motion of polymer chain segments. Upon nanofiller incorporation, the peak shifted slightly upward: ~87 °C for 0.5C, ~91 °C for 1.0C, and ~89 °C for 2.0C, indicating that the glass transition temperature ($T_g$) increases with nanocarbon addition.

In addition, the intensity of the E″ peak increased with nanofiller content up to 1.0 wt%, reflecting greater energy dissipation. This enhancement is linked to increased interfacial friction and restricted chain dynamics at the polymer–filler boundary, which promote viscoelastic damping. At 2.0 wt%, however, the E″ peak intensity slightly decreased, again suggesting the onset of filler agglomeration that reduces effective chain–filler interactions. These findings confirm that carbon nanostructures influence the relaxation dynamics and enhance energy dissipation, consistent with prior reports on nanofilled polymers [29].

Also shown in Figure 4(b) (dashed curves), tan δ provides a direct measure of damping efficiency and interfacial interactions. Neat PVA exhibited a sharp tan δ peak at ~85 °C, whereas nanocomposites shifted upward to ~87–91 °C, confirming the $T_g$ rise due to restricted chain segmental mobility. Importantly, the tan δ peak height decreased with nanofiller incorporation: neat PVA exhibited the highest damping, while PVA–1.0C and PVA–2.0C showed progressively lower maxima.

A reduced tan δ peak implies lower energy dissipation and stronger interfacial adhesion between polymer chains and nanofillers. This is desirable for structural and thermal stability under cyclic solar heating, as it means the material stores more elastic energy and resists deformation [30].

**Thermal Transport Behaviour (TPS Analysis)**

The thermal transport properties of neat PVA and PVA–carbon nanocomposites were presented in Figure 4, where thermal conductivity (k), thermal diffusivity (α), and retention after 10 thermal cycles are combined in a single multi-axis plot for clarity. This integrated representation allows direct comparison of the effects of nanofiller loading on instantaneous heat transport and long-term stability.

From Figure 5, it is evident that neat PVA starts with a baseline conductivity of ~0.25 $W \cdot m^{-1} \cdot K^{-1}$ and diffusivity of ~0.12 $mm^2 \cdot s^{-1}$, values typical of semi-crystalline insulating polymers with limited phonon mobility across amorphous–crystalline boundaries. Upon nanofiller incorporation, both k and α increased significantly, were reflecting the formation of percolative filler networks that enhance phonon conduction pathways. At 1.0 wt%, k rose to ~0.58 $W \cdot m^{-1} \cdot K^{-1}$ and α to ~0.26 $mm^2 \cdot s^{-1}$, while 2.0 wt% reached ~0.72 $W \cdot m^{-1} \cdot K^{-1}$ and ~0.31 $mm^2 \cdot s^{-1}$, respectively. This ~3-fold improvement in k demonstrates the critical role of synergistic graphene–CNT frameworks in bridging interfacial voids, minimizing phonon scattering, and enabling efficient energy transfer [16–18].

Interestingly, the curvature of both k and α trends highlights an important balance: while higher filler loadings improve heat conduction, excessively high conductivity may promote undesirable bulk heat dissipation rather than interfacial heat localization. This trade-off is clearly visible in Figure 4, where the optimum lies around 1.0 wt%—sufficient to accelerate interfacial evaporation under solar irradiation while preventing thermal leakage into the bulk water reservoir [19].

 

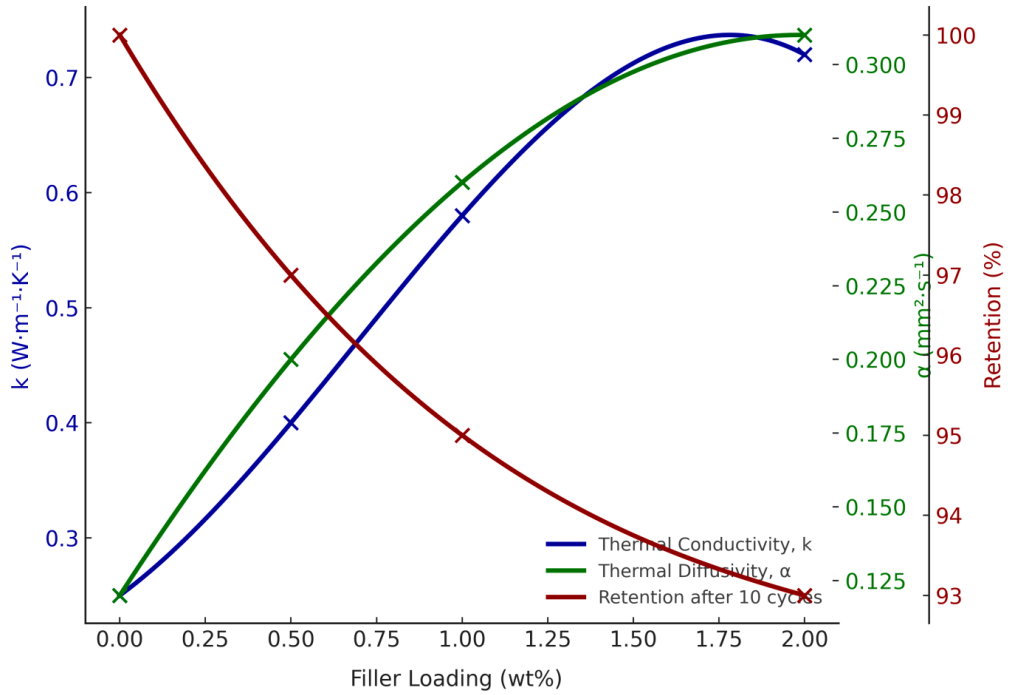


**Figure 5.** TPS thermal transport properties of neat PVA and nanocomposites: thermal conductivity (k), thermal diffusivity (α), and retention after 10 cycles versus filler loading

The same figure 5 also depicts the retention of k and α values after 10 thermal cycles (25–80 °C). All compositions retained more than 93% of their original performance, with neat PVA maintaining 100% and the nanocomposites stabilizing around 93–97%. The smooth maroon retention curve confirms the long-term durability of polymer–filler interfaces, indicating no interfacial debonding, phase segregation, or microcrack formation during cyclic thermal stresses. This durability is particularly critical for real-world solar water purification systems, where the films are subjected to repeated heating–cooling cycles [20].

## CONCLUSION

The present study demonstrated that carbon nanostructure-reinforced PVA nanocomposites exhibit enhanced thermo-mechanical and solar-relevant performance. Based on the obtained results, the following key conclusions were derived:

- Tensile strength increased from ~38 MPa (neat PVA) to ~52 MPa at 1.0 wt% loading, showing optimum reinforcement.
- Young's modulus improved from ~0.9 GPa to ~1.3 GPa, while elongation remained acceptable (~135%), ensuring flexibility.
- Tg increased by ~7 °C, while crystallinity decreased by ~11%, promoting heat absorption efficiency.
- Storage modulus rose by ~50% at 1.0 wt%, confirming superior stiffness and dimensional stability.
- Thermal conductivity and diffusivity improved nearly threefold, reaching ~0.72 $W \cdot m^{-1} \cdot K^{-1}$ and ~0.31 $mm^2 \cdot s^{-1}$, respectively.
- Thermal transport retention remained above 93% after 10 heating cycles, highlighting long-term reliability.

These outcomes collectively establish 1.0 wt% nanofiller loading as the most effective balance for mechanical durability, thermal responsiveness, and energy localization, thereby underscoring the potential of these nanocomposites for scalable solar-driven water purification.

 

## REFERENCES


1. Galpaya D, Wang M, Liu M, Motta N, Waclawik E, Yan C. Recent advances in fabrication and characterization of graphene-polymer nanocomposites. Graphene. 2012;1:30-49.
2. Xiao M, Sun L, Liu J, Li Y, Gong K. Synthesis and properties of polystyrene/graphite nanocomposites. Polymer. 2002;43:2245-8.
3. Tang LC, Wan YJ, Yan D, Pei YB, Zhao L, Li YB, et al. The effect of graphene dispersion on the mechanical properties of graphene/epoxy composites. Carbon. 2013;60:16-27.
4. Ferrari AC. Raman spectroscopy of graphene and graphite: Disorder, electron–phonon coupling, doping and nonadiabatic effects. Solid State Commun. 2007;143:47-57.
5. Park JK, Do IH, Askeland P, Drzal LT. Electrodeposition of exfoliated graphite nanoplatelets onto carbon fibers and properties of their epoxy composites. Compos Sci Technol. 2008;68:1734-41.
6. Li J, Vaisman L, Marom G, Kim JK. Br treated graphite nanoplatelets for improved electrical conductivity of polymer composites. Carbon. 2007;45:744-50.
7. Zope IS, Dasari A. High-temperature-resistant polymer nanocomposites. In: Functional and Physical Properties of Polymer Nanocomposites. Hoboken: John Wiley & Sons; 2016. p.183-201.
8. Paredes JI, Villar-Rodil S, Fernández-Merino MJ, Guardia L, Martínez-Alonso A, Tascón JMD. Environmentally friendly approaches toward the mass production of processable graphene from graphite oxide. J Mater Chem. 2011;21:298-306.
9. Jayasena B, Melkote SN. An investigation of PDMS stamp assisted mechanical exfoliation of large area graphene. Procedia Manuf. 2015;1:840-53.
10. King JA, Klimek DR, Miskioglu I, Odegard GM. Mechanical properties of graphene nanoplatelet/epoxy composites. J ApplPolym Sci. 2012;128:4217-23.
11. Liao L, Lin YC, Bao M, Cheng R, Bai J, Liu Y, et al. High-speed graphene transistors with a self-aligned nanowire gate. Nature. 2010;467:305-8.
12. Scognamiglio F, Mirabile Gattia D, Roselli G, Persia F, De Angelis U, Santulli C. Thermoplastic starch films added with dry nopal (Opuntia ficus indica) fibers. Fibers. 2019;7:99.
13. Battegazzore D, Noori A, Frache A. Natural wastes as particle filler for poly(lactic acid)-based composites. J Compos Mater. 2019;53(6):783–97.
14. Rizalludin MHM, Sapuan SM, Rodzi MNM, Ibrahim MS, Sherwani SFK. A review of seaweed based composites. Compos Aquat Environ. 2023;315–37.
15. Berthet MA, Angellier-Coussy H, Guillard V, Gontard N. Vegetal fiber-based biocomposites: which stakes for food packaging applications? J ApplPolym Sci. 2016;133(2):42528.
16. Kulhan T, Kamboj A, Gupta NK, Somani N. Fabrication methods of glass fibre composites—A review. Funct Compos Struct. 2022;4(2):022001.
17. Das O, Kim NK, Hedenqvist MS, Lin RJT, Sarmah AK, Bhattacharyya D. An attempt to find a suitable biomass for biochar-based polypropylene biocomposites. Environ Manag. 2018;62:403–13.
18. Abba HA, Nur IZ, Salit SM. Review of agro waste plastic composites production. J Miner Mater Charact Eng. 2013;1(5):271–9.
19. Ruiz JM, Marco-Méndez C, Sánchez-Lizaso JL. Remote influence of off-shore fish farm waste on Mediterranean seagrass (Posidonia oceanica) meadows. Mar Environ Res. 2010;69:118–26.
20. Dumee LF, et al. Activation of gold decorated carbon nanotube hybrids for targeted gas adsorption and enhanced catalytic oxidation. Prog Nat Sci Mater Inter. 2012;22:673-83.
21. Mittal G, Dhand V, Rhee KY, Park SJ, Lee WR. A review on carbon nanotubes and graphene as fillers in reinforced polymer nanocomposites. J Ind Eng Chem. 2014;21:11-25.
22. Wu Y, Lin YM, Bol A, Jenkins KA, Xia F, Farmer DB, et al. High-frequency, scaled graphene transistors on diamond-like carbon. Nature. 2011;472:74-8.
23. Kim KS, Zhao Y, Jang H, Lee SY, Kim JM, Kim KS, et al. Large-scale pattern growth of graphene films for stretchable transparent electrodes. Nature. 2009;457:706-10.
24. Zhao X, Zhang Q, Chen D, Lu P. Enhanced mechanical properties of graphene-based poly(vinyl alcohol) composites. Macromolecules. 2010;43:2357-63.


 

25. Hameed N, et al. Individual dispersion of carbon nanotubes in epoxy via a novel dispersion–curing approach using ionic liquids. Phys Chem Chem Phys. 2013;15:11696-703.
26. Almeshaal M, Palanisamy S, Murugesan TM, Palaniappan M, Santulli C. Physico-chemical characterization of Grewia monticolaSond (GMS) fibers for prospective application in biocomposites. J Nat Fibers. 2022;19(17):15276–90. doi:10.1080/15440478.2022.2123076.
27. Santulli C, Palanisamy S, Mayandi K. Pineapple fibers, their composites and applications. In: Advances in Natural Fibre Composites. Elsevier; 2022. doi:10.1016/B978-0-12-824528-6.00007-2.
28. Palaniappan M, Palanisamy S, Khan R, et al. Synthesis and suitability characterization of microcrystalline cellulose from Citrus × sinensis sweet orange peel fruit waste-based biomass for polymer composite applications. J Polym Res. 2024;31:105. doi:10.1007/s10965-024-03946-0.
29. Goutham ERS, Hussain SS, Muthukumar C, Krishnasamy S, Kumar TSM, Santulli C, Palanisamy S, Parameswaranpillai J, Jesuarockiam N. Drilling parameters and post-drilling residual tensile properties of natural-fiber-reinforced composites: A review. J Compos Sci. 2023;7(4):136. doi:10.3390/jcs7040136.
30. Karuppusamy M, Thirumalaisamy R, Palanisamy S, Nagamalai S, Massoud E. A review of machine learning applications in polymer composites: advancements, challenges, and future prospects. J Mater Chem A. 2025;13. doi:10.1039/D5TA00982K.

 